

Characterization and Implementation of Resonant Isolated DC/DC Converters for Future MVdc Railway Electrification Systems

Joseph Fabre^{ID}, Philippe Ladoux^{ID}, Member, IEEE, Hervé Caron, Andrea Verdicchio^{ID}, Jean-Marc Blaqui  re, Didier Flumian, and S  bastien Sanchez^{ID}

Abstract—Today, in electric railways, the old dc supply systems are reaching their limits. To improve their efficiency and increase railroad traffic, a new dc electrification has recently been proposed at 9 kV. It is now necessary to prepare the migration of infrastructure and rolling stock, using power electronic transformers (PETs), for adaptation to this voltage level. For this application, high efficiency and reduced volume are essential. This article clearly demonstrates that it is now possible to achieve a compact, high-power, isolated dc-dc converters using 3.3-kV SiC-MOSFET power modules with high efficiency. After a preliminary study based on simulations, this article focuses on the characterization and implementation of elementary isolated dc-dc converters. The proposed topology is a series-resonant converter rated for a nominal power of 300 kW at 1.8 kV. First, laboratory testing using an “opposition method” is used to evaluate the elementary converters up to their nominal power using both electrical and thermal measurements to accurately determine losses and efficiency. At the nominal output power, an efficiency of 98.93% is obtained. This is quite remarkable for an isolated dc-dc converter operating under 1.8 kV with a switching frequency of 15 kHz. Finally, two elementary isolated dc/dc converters are associated with input series/output parallel (ISOP) configuration in order to achieve a 3-kV/1.5-kV PET with a nominal power of 600 kW as a prelude to the final 9/1.5-kV power conversion.

Index Terms—DC-DC power converters, loss measurement, power MOSFET, rail transportation, silicon carbide, traction power supplies.

I. INTRODUCTION

FOR various historical reasons, in Europe today, several railway electrification systems are in use dc power supplies at 1.5 or 3 kV and ac power supplies at 15 kV/16.7 Hz or 25 kV/50 Hz [1], [2]. Due to the increase in regional and freight traffics, more and more traction power is required.

Manuscript received May 12, 2020; revised July 21, 2020 and September 21, 2020; accepted October 18, 2020. Date of publication October 28, 2020; date of current version May 10, 2021. This work was supported by the French National Railway Company [Soci  t   Nationale des Chemins de Fer Fran  ais (SNCF)]. (Corresponding author: Joseph Fabre.)

Joseph Fabre, Philippe Ladoux, Jean-Marc Blaqui  re, Didier Flumian, and S  bastien Sanchez are with the Laboratoire Plasma et Conversion d’Energie (LAPLACE), 聂cole Nationale Sup  rieure d’Electrotechnique, d’Electronique, d’Informatique, d’Hydraulique et des T  l  communications (ENSEEIHT), Institut National Polytechnique de Toulouse (INPT), 31071 Toulouse, France (e-mail: joseph.fabre@laplace.univ-tlse.fr; philippe.ladoux@laplace.univ-tlse.fr; jean-marc.blaquier@laplace.univ-tlse.fr; didier.flumian@laplace.univ-tlse.fr; sebastien.sanchez@laplace.univ-tlse.fr).

Herv   Caron and Andrea Verdicchio are with French National Railway Company (SNCF), 93210 Saint-Denis, France (e-mail: herve.caron@reseau.sncf.fr; ext.andrea.verdicchio@sncf.fr).

Digital Object Identifier 10.1109/TTE.2020.3033659

The dc power systems suffer from the relatively low-voltage levels that draw high currents, and in order to avoid an excessive line-voltage drop, the distance between substations must be minimized, and the overhead lines must have a large cross section. For example, at 1.5-kV dc, it is not uncommon to find overhead-line cross sections of up to 1000 mm² and a substation spacing of around 15 km. Thus, the mechanical infrastructure of the overhead line is heavy and expensive, whereas the onboard traction converter of a dc locomotive is simple and reduced to an input filter and a three-phase voltage-source inverter [3].

On the other hand, lines electrified in ac benefit from higher voltage levels and lower overhead-line cross sections. Nevertheless, ac operation entails reactive power and, therefore, inductive voltage drops [4], [5]. In the 25-kV/50-Hz system, the substations are only based on a single-phase transformer, but, in order to rebalance the power on the upstream three-phase transmission lines, the substations are supplied by different phases. As a result, the railway line is divided into sectors that are isolated by neutral sections [6], so the substations are never connected in parallel and require high short-circuit power at the coupling point to avoid voltage imbalances. Also, ac traction chains are more complex than those using dc since modern locomotives include a single-phase step-down transformer, an active front-end rectifier (four-quadrant rectifier), a low-frequency filter to mitigate the fluctuating power (33.3 or 100 Hz) on the dc bus, and a three-phase voltage-source inverter that supplies the ac traction motor [3].

In recent years, the attractiveness of medium-voltage dc (MVdc) networks compared with MVac power systems has grown steadily. The potential applications are mainly onboard electrical networks for ship propulsion, offshore wind farms, or smartgirds [7]–[9], and it is clear that, in the future, MVdc power grids will contribute to the deployment of renewable energy sources and associated storage systems, as well as charging stations for electric vehicles.

Regarding the breaking of dc fault currents, several projects, in particular for HVDC grids, have led to the development of hybrid circuit breakers (CRs) (semiconductors and mechanical switch) [10]–[12]. Meanwhile, on the power converter side, multilevel voltage-source inverters are already used in variable speed MV drives for industrial motors operating from 6 to 10 kV [13].

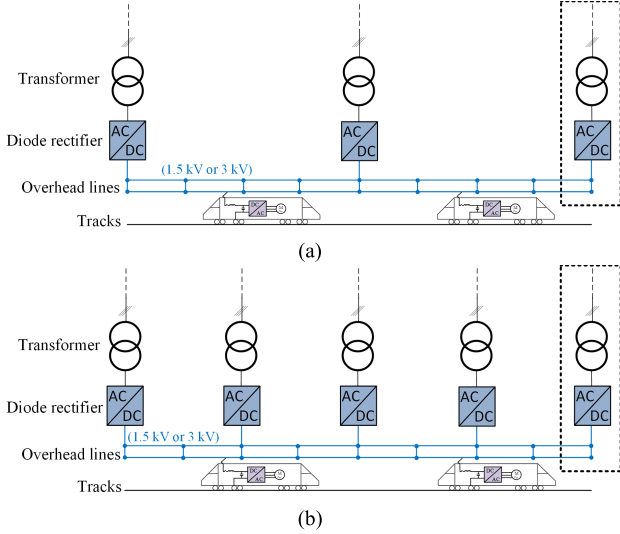


Fig. 1. Classical solution to increase the railroad traffic in a railway line electrified in dc (1.5 or 3 kV). (a) Initial situation. (b) Installation of new intermediate substations.

In this context, French National Railway Company (SNCF) is decided to investigate the possibility of increasing the voltage on dc railway lines and in 2018, a new 9-kV dc railway electrification system was proposed. In the article [8], it was shown that, in the case of high-speed lines, this power system offers identical performances to the 2×25 kV ac system while reducing the power installed in substations. In addition, SNCF launched a study aimed at upgrading their 1.5-kV dc lines to 9-kV dc. In particular, the article [14] presented a strategy consisting of introducing a 9-kV dc power transmission line in parallel with the 1.5-kV dc overhead line. Fig. 1(a) and (b) shows, respectively, the initial situation of electrification at 1.5-kV dc and the conventional reinforcement solution based on intermediate substations where it is necessary to make new connections to the public grid.

A progressive migration to a 9-kV system is presented in Fig. 2. To supply a voltage of 9 kV, ac/dc rectifiers are installed in some substations. The intermediate substations are replaced by step-down power electronic transformers (PETs) that supply power to the railway line without changing the operating voltage of the rolling stock. These PETs will be developed in the form of easily relocatable containers. In the final step, the overhead line will be totally renewed (new catenaries with a reduced cross section and lighter support posts) and directly supplied in 9-kV dc. The PETs will be dismounted and assigned to another line being transformed, while, at the same time, the rolling stock will be adapted to this voltage level. In the case of existing traction units, this can be achieved by introducing a step-down PET onboard [15], [16]. For a new fleet of vehicles, a new traction chain operating directly under 9-kV dc could be based on multilevel inverters [7], [17], [18] and medium-voltage traction motors [13].

Furthermore, in the context of sustainable development and the evolution of a global energy mix, the choice of an MVdc power system offers a new opportunity for railway lines: they can now act as energy hubs by facilitating the connection

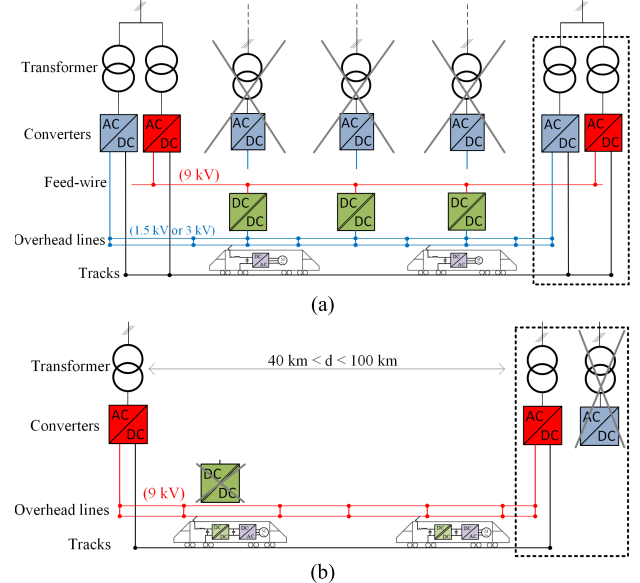


Fig. 2. (a) Intermediate electrification system: three-wire supply system with a 9-kV feed wire. (b) Final stage: 9-kV dc electrification system.

of distributed renewable energy sources along the track and integrating energy-storage devices in accordance with Fig. 3.

The rail network operator can, thus, sell services other than the transport of passengers and freight. For example, in periods of low railroad traffic, due to its storage elements [19], the “smart” rail network can support the public grid and contribute to primary frequency control [20].

In all the cases mentioned earlier, PETs will evidently play an essential role, but, first, the feasibility of such devices at power levels of several megawatts must be investigated and demonstrated. Therefore, after a preliminary study based on electrothermal simulation on the PLECS software, this article focuses on the characterization and implementation of an isolated dc/dc converter based on a resonant-single-active-bridge topology (R-SAB) using 3.3-kV SiC MOSFET modules. This converter, with a nominal power of 300 kW, is sized to operate at 15 kHz and 1.8 kV. An opposition method is proposed to test this converter. Electrical and thermal measurements are used to accurately determine losses and efficiency. Different solutions for the output rectifier are evaluated: Si-diodes, SiC-diodes, or SiC MOSFETs in synchronous rectifier operation. Finally, two elementary converters are associated with the input series/output parallel (ISOP) configuration in order to evaluate the performance of a 3-/1.5-PET.

II. DC-DC ISOLATED CONVERTERS

A. Considerations on SiC MOSFET Power Modules

The manufacturing processes for SiC components are complex, but, in these last years, considerable advances were made. At the same time, a new recommendation from the Roll2Rail community has led to improved packaging of power modules for the rail sector [21]. These new packages, called “low-voltage module” (LVM; $V_{CES} \leq 3.3$ kV) and “high-voltage module” (HVM; $V_{CES} \geq 3.3$ kV), are proposed now by several manufacturers [22]–[29].

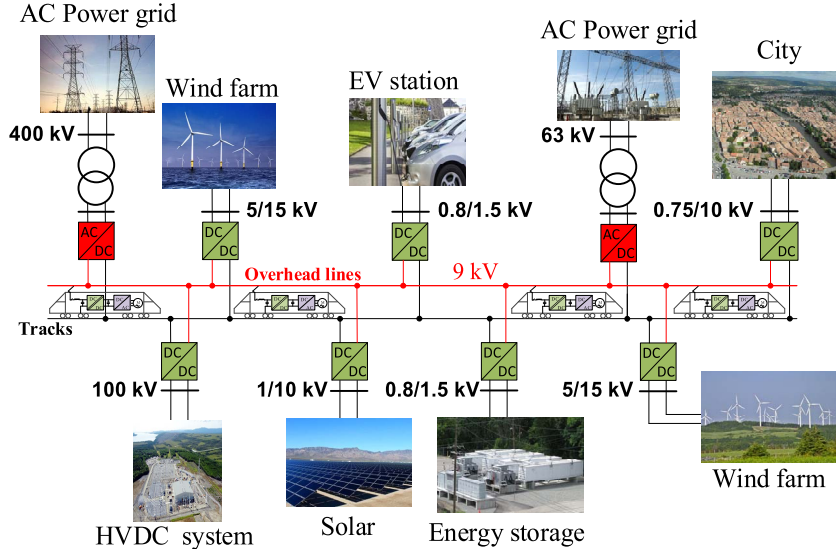


Fig. 3. Concept of a future railway MVdc smart grid.

In 2019, the first 3.3-kV SiC-MOSFET power modules [23], [24] became available, and this made it possible to consider the design of high-voltage and high-power converters with high switching frequencies while maintaining compactness and efficiency [30]–[33]. These advantages are essential for our application where PETs have to be installed in a reduced space whether in preexisting substations or onboard rolling stock [34]. Nevertheless, the low availability and the high cost of these new power modules mean that the number of publications concerning their use in power converters is quite small. Moreover, in the datasheets provided by the manufacturers, there is no information concerning the energy losses in soft-switching, which does not facilitate converter design. That is why the article [35] presented a specific gate driver allowing zero-voltage switching (ZVS) operation of 3.3-kV SiC MOSFET modules and showed measurements of switching energies.

B. Considerations on Medium-Frequency Transformer Design

Beyond the adaptation of the level of voltage and current between the primary and secondary circuits, the transformer has a role of galvanic isolation between two power systems. In order to decrease the size and weight of a transformer, it is necessary to increase its operating frequency. However, this is only possible through the use of dedicated magnetic materials [36] and by fine calculations of electric, magnetic, and thermal fields [37]–[39]. The control of electrical parameters, such as winding capacitances, magnetizing, and leakage inductances, while respecting the choice of the turns ratio, is, therefore, essential. Especially, since the overall reduction in size increases the challenges from a dielectric point of view, in this article, the design of the MFT relies on the know-how of ABB Secheron Ltd., which has extensive experience in this field. The article [40] presents the design of a 1.2-MW PET demonstrator for traction applications with a transformer operating at a frequency of around 2 kHz. The article [41] presents

the design and the experimental results of a 100 kW and 30 kV insulated MFT operating at 22 kHz, which is technologically close to that used in the isolated dc/dc converter presented in this article (Nanocrystalline magnetic core and litz windings).

C. 9-kV/1.5-kV PET Choice of the Converter Topology

As developed in Section I, the PET is an essential device for the progressive implementation of a new MVdc electrification system in railways. For safety reasons, galvanic isolation between the 9- and 1.5-kV voltage levels is mandatory. This excludes different topologies of multilevel choppers, such as the flying capacitor topology [42] or triangular structures [43], [44]. Thus, two topologies can be considered: the isolated modular multilevel converter (IMMC) [7], [45], [46] and the Association of Isolated DC/DC Converters (AIDC) in the ISOP configuration [17], as presented in Fig. 4(a) and (b), respectively.

The IMMC requires a single transformer and can be applied to high-voltage and high-power applications, such as in the interconnection of HVDC grids. In this case, a classical construction of an oil-filled transformer is used (large insulator bushings and magnetic core with laminated silicon steel). Nevertheless, the operating frequency should then be reduced to a few kHz in order to avoid excessive core losses. On the other hand, AIDC requires several transformers that can operate at higher frequencies (a few tens of kHz). Nevertheless, as mentioned in Section II-B, due to its small size, the realization of the transformer is a critical issue (power density, creepage distance, and winding insulation). As a result, this topology will be limited to applications where the operating voltage does not exceed a few tens of kV.

In the article [7], a comparative study between IMMC and AIDC topologies for an HVDC off-shore wind-farm application was presented. This study was only based on calculations and simulation results. In particular, 3.3-kV SiC MOSFET power modules were considered. Finally, the results

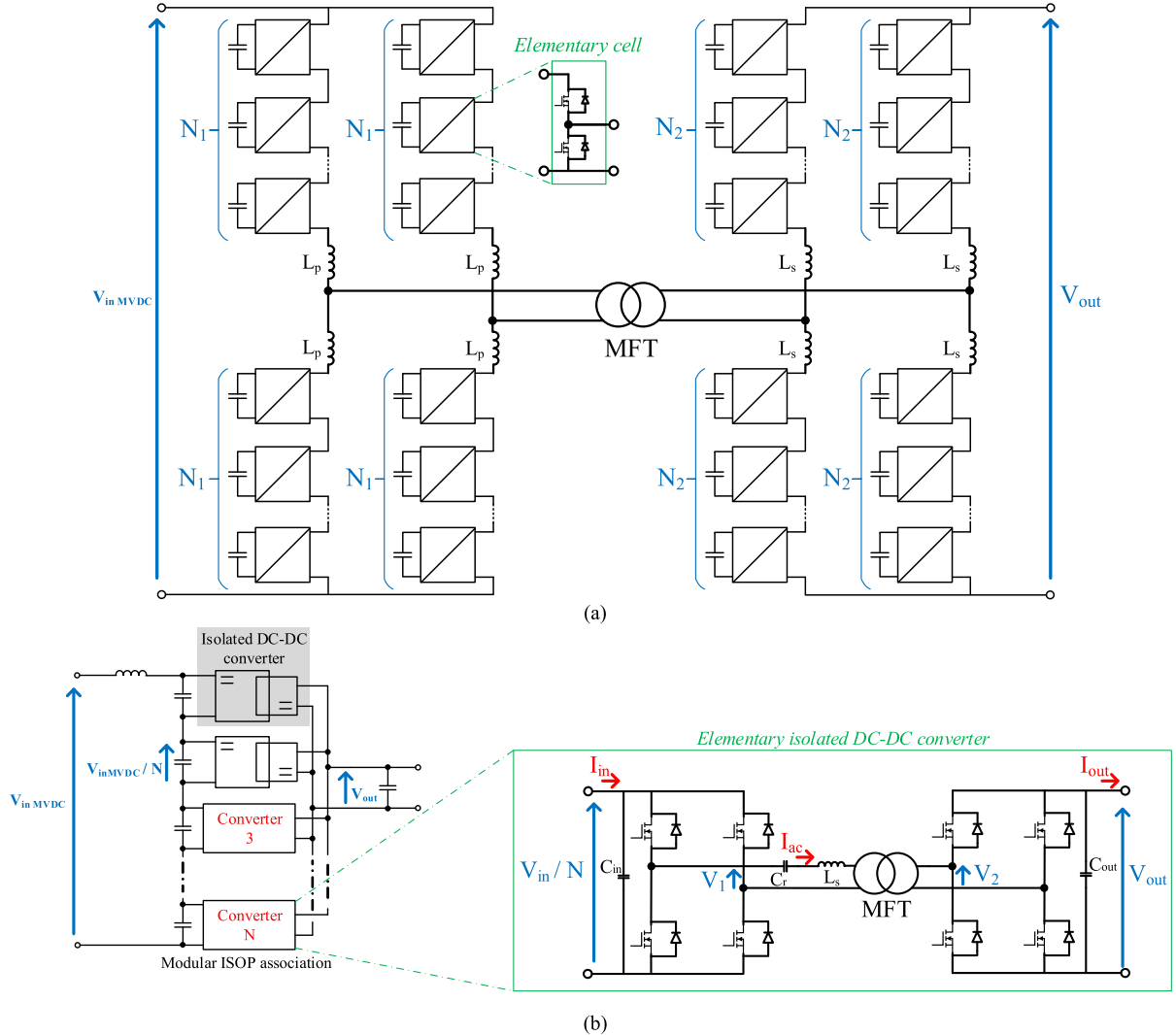


Fig. 4. Two isolated topologies. (a) IMMC. (b) Association of Isolated DC/DC Converters (AIDC) in the ISOP configuration.

showed that AIDC is attractive in view of the minimal energy stored in the dc filtering capacitors. Furthermore, from an efficiency viewpoint, the AIDC showed minimally lower loss than the IMMC. In terms of control, the IMMC requires a specific algorithm to balance the voltage on the capacitors, and each elementary cell has to include a voltage sensor. On the other hand, in the AIDC, due to the ISOP configuration, voltage and current balancing is natural, and as a result, no specific control algorithm is required. In the application considered in this article (9-/1.5-kV dc/dc conversion) despite the fact that the transformer is small, galvanic isolation is not problematic because the required isolation level is only 20 kV ($\approx 9 \text{ kV} \times 2 + 1 \text{ kV}$) according to transportation standards. Thus, considering all these statements, the AIDC topology was selected.

Finally, Fig. 5(a) shows a possible solution for the intermediate electrification system where the converter between the 9-kV feed wire and the 1.5-kV overhead line is based on an ISOP association of elementary isolated dc-dc converters. With a SiC MOSFET voltage rating of 3.3 kV, the number N of elementary converters is set to 6. As shown in Fig. 5(b),

the same structure can be used to adapt an existing traction chain to the MVdc power supply. The PET is then positioned upstream of the traction inverter which continues to operate with a 1.5-kV dc bus.

III. STUDY AND SIMULATION OF THE RESONANT ISOLATED DC/DC CONVERTERS

A. Introduction

Several studies have been carried out [47], [40], in the field of railway electric traction over the last ten years, concerning the topology of elementary isolated dc/dc converters, with the goal of replacing the input transformer of locomotives operating on ac power lines (25 kV/50 Hz or 15 kV/16.7 Hz).

Considering the characteristics of silicon devices (6.5-kV IGBTs), these studies have highlighted that a resonant topology, as shown in Fig. 6, is well suited. Indeed, the total leakage inductance of the transformer (L_s) is associated with a series capacitor (C_r) to form a resonant circuit. Resonance frequency f_0 is then chosen to obtain a sinusoidal waveform for the current in the ac link and provide a soft-switching

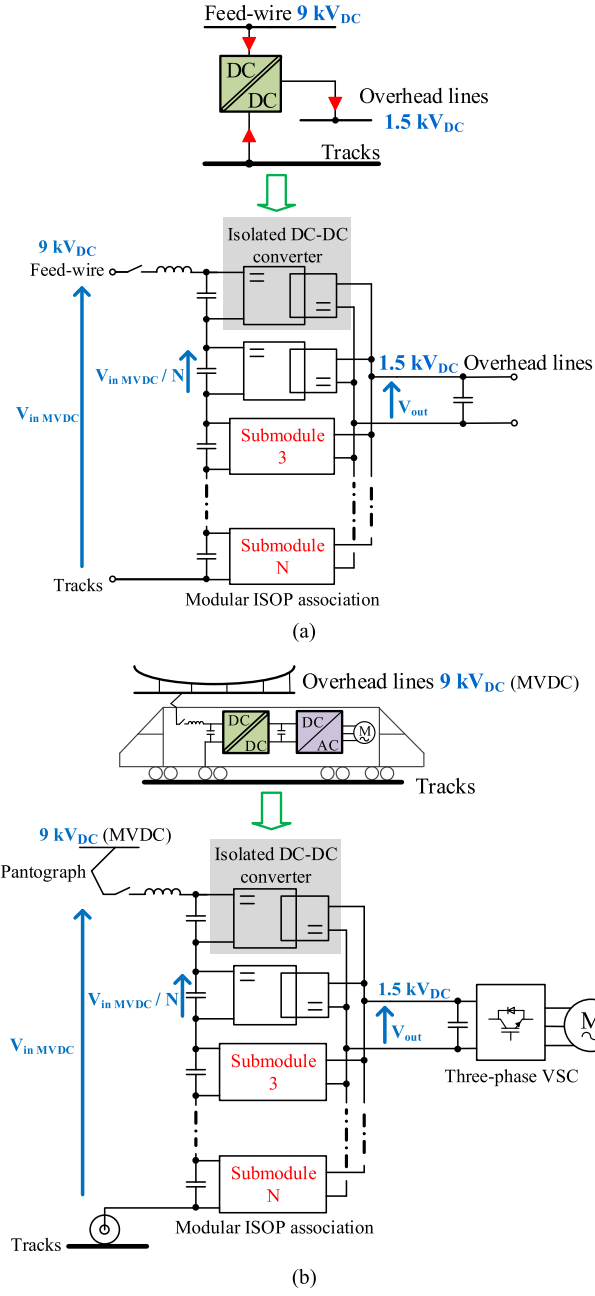


Fig. 5. Structure of the isolated dc-dc converter consisting of N elementary blocks in the ISOP association. (a) Converter between the feed wire and the overhead lines (intermediate electrification system). (b) Adaptation converter of the current traction chain to the 9-kV dc network.

operation of the transistors and the diodes, thus reducing the switching losses. As a result, with high-voltage devices, it is possible to achieve a switching frequency much higher than that commonly used in hard-switching.

The availability of high-voltage SiC devices makes it possible to achieve high-efficiency isolated dc/dc converter operation with a switching frequency f_{sw} above 10 kHz. This allows, on the one hand, transformer size reduction and, on the other hand, acoustic noise reduction. Even if recent work has demonstrated the advantages of SiC devices in this application [7], [18], [35], it was, nevertheless, important to

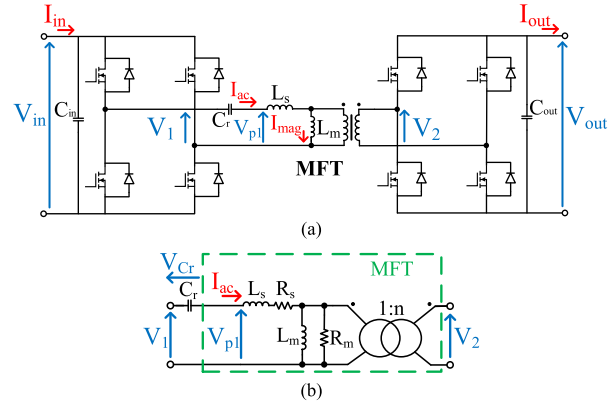


Fig. 6. Resonant Dual H-Bridge converter. (a) Topology of the isolated dc/dc converter. (b) High-frequency link equivalent-circuit (series resonant capacitor and MFT).

TABLE I
PARAMETERS OF THE MEDIUM-FREQUENCY TRANSFORMER $V_{in} = 1800\text{ V}$, $f_{sw} = 15\text{ kHz}$, TURNS RATIO 1:1, $S_{MFT} \approx 400\text{ kVA}$, AND $I_{ac} \approx 223\text{ A}$

Magnetizing inductance (L_m)	5.7 mH
Total leakage inductance of the transformer (L_s)	22.5 μH
Total equivalent series resistances of the transformer (R_s)	17.5 m Ω
Core loss equivalent resistance (R_m)	7.9 k Ω

build a prototype at a significant power level in order to better understand the constraints of using these new devices and accurately measure system efficiency. This prototype is based on 3.3-kV/750-A SiC-MOSFET modules from Mitsubishi [23], [24] and a water-cooled medium-frequency transformer (MFT) made by ABB Secheron Ltd. [41].

To prepare the design of this prototype, considering the characteristics of the MFT, a preliminary sizing study of the resonant circuit has been carried out. Then, simulations with PLECS software were carried out with the view to assess the losses and choose the converter operating mode leading to the best efficiency.

B. Sizing of the Series-Resonance Circuit

1) *Choice of Resonance Frequency and Converter Operating Mode:* A preliminary design of a 400-kVA transformer rated for a frequency of 15 kHz and a nominal voltage of 1.8 kV was performed by ABB Secheron Ltd. The parameters are given in Table I.

For the resonant dual H-bridge topology, as presented in Fig. 6, three modes of operation were considered. For all cases, taking into account the switching behavior of the SiC MOSFETs, a ZVS operation is chosen (controlled turn-off and spontaneous turn-on at zero voltage crossing). In the resonant-dual-active-bridge (R-DAB) mode, the two H-Bridges are simultaneously controlled, and the phase shift of voltages

V_1 and V_2 controls the power flow in order to regulate the output voltage V_{out} [7]. The ZVS operation is achieved by choosing a switching frequency f_{sw} higher than the resonance frequency f_0 . Nevertheless, this operating mode leads to having switching losses in both H-Bridges. To improve the efficiency of the converter, it can be interesting to have controlled commutations only on one H-Bridge, the second H-bridge working as a diode rectifier. This mode is called R-SAB operation. In this case, the output characteristic of the dc/dc converter is similar to that of a voltage source with an internal resistance depending on the impedance of the ac stage (transformer winding resistance, leakage inductance, and series resonance capacitor). The output power of the converter only depends on the load consumption, and no output voltage control is required (open-loop operation). If f_0 is lower than f_{sw} , a continuous conduction mode (CCM) is obtained. On the contrary, if f_0 is higher than f_{sw} , a discontinuous conduction mode (DCM) results. In this case, the MOSFET turn-off losses theoretically depend only on the magnetizing current of the transformer.

2) *Capacitor Sizing for R-DAB and R-SAB CCM:* For the operations in R-DAB and R-SAB CCM, the frequency ratio (f_{sw}/f_0) was set at 1.4 in order to ensure sufficiently selective filtering of the current in the transformer while limiting the capacitor voltage.

For the R-DAB operation, the impedance of the series-resonance circuit has to be high enough to guarantee proper controllability of the output current and the ZVS mode over the operating range of the converter. As a result, the phase shift angle δ was set to 40° for the nominal output current, which leads to having a series-resonance circuit impedance of 5.5Ω . Thus, the total inductance of the series-resonance circuit must have a value of $120 \mu\text{H}$, which requires placing an additional inductor outside the transformer. For the R-SAB operation in CCM, to limit the on-load voltage drop, the impedance of the series-resonance circuit has to be minimum, and only the leakage inductor of the transformer is used. All equations were established by assuming the current i_{ac} to be perfectly sinusoidal.

The rms value of the current in the resonant capacitor I_{ac} versus output current I_{out} is given by (1). In the case of the R-SAB CCM, δ must be considered as zero

$$I_{\text{ac}} = \frac{\pi}{2\sqrt{2}} \cdot \frac{I_{\text{out}}}{\cos(\frac{\delta}{2})}. \quad (1)$$

Equations (2) and (3) allow calculating the rms voltage V_{C_r} and the reactive power Q_{C_r} , respectively

$$V_{C_r} = \frac{I_{\text{ac}}}{2\pi f_{\text{sw}} C_r} \quad (2)$$

$$Q_{C_r} = V_{C_r} \cdot I_{\text{ac}}. \quad (3)$$

3) *Capacitor Sizing for R-SAB DCM:* In order to ensure the DCM, the switching frequency should be lower than the resonance frequency. In our case, the frequency ratio (f_{sw}/f_0) was set at 0.78 in order to obtain a sufficient turn-off time to allow the proper recovery of the diodes with a low reverse blocking voltage.

TABLE II
RESONANT CAPACITOR SIZING FOR THE THREE OPERATING MODES OF THE RESONANT ISOLATED DC-DC CONVERTER $V_{\text{in}} = 1800 \text{ V}$, $f_{\text{sw}} = 15 \text{ kHz}$, TURNS RATIO 1:1, $I_{\text{out}} = 170 \text{ A}$

	R-DAB	R-SAB CCM	R-SAB DCM
Total series inductance	$120 \mu\text{H}$	$22.5 \mu\text{H}$	$22.5 \mu\text{H}$
Frequency ratio (f_{sw}/f_0)	1.4	1.4	0.78
Resonance frequency (f_0)	10.8 kHz	10.8 kHz	19.4 kHz
Series capacitor (C_r)	$1.8 \mu\text{F}$	$9.6 \mu\text{F}$	$3 \mu\text{F}$
RMS current (I_{ac})	$201 \text{ A}_{\text{rms}}$	$188.9 \text{ A}_{\text{rms}}$	$213.8 \text{ A}_{\text{rms}}$
RMS voltage (V_{C_r})	$1184.8 \text{ V}_{\text{rms}}$	$207.7 \text{ V}_{\text{rms}}$	$738.8 \text{ V}_{\text{rms}}$
Reactive power (Q_{C_r})	238.1 kVAR	39.2 kVAR	158 kVAR

Equations (4) and (5) were established by considering that, during the conduction of the diodes, current i_{ac} shows a half-sine waveform at frequency f_0 .

The rms value of the current in the series-resonance capacitor I_{ac} versus output current I_{out} is given by the following equation:

$$I_{\text{ac}} = \frac{\pi}{2\sqrt{2}} \cdot \sqrt{\frac{f_0}{f_{\text{sw}}}} \cdot I_{\text{out}}. \quad (4)$$

Equation (5) allows calculating the rms value of the voltage across the capacitor. Reactive power Q_{C_r} is calculated by (3)

$$V_{C_r} = \frac{I_{\text{ac}}}{2\pi f_0 C_r} \cdot \sqrt{\left(2 \cdot \frac{f_0}{f_{\text{sw}}} - 1\right)}. \quad (5)$$

The calculation results are presented in Table II.

C. PLECS Thermal Model of the Resonant Isolated DC/DC Converter

In the simulation circuit, PLECS consider an ideal switch model. To calculate the semiconductor losses, PLECS records the semiconductor's operating condition before and after each switch operation. It then uses these parameters to read the resulting dissipated energy from a 3-D lookup table considering switched current, blocking voltage, and junction temperature. During the ON-state, the dissipated power is computed from the device current and temperature. This combination of ideal switch models with detailed loss data provides an efficient and accurate alternative to detailed device simulations. The required data tables are entered via an integrated visual editor from the manufacturer's datasheet. Once the dissipated power is calculated, the thermal model is used to compute the junction temperature of the device. Thus, PLECS software performs an iterative calculation to obtain the operating point in a steady state. Table III shows the electrical and thermal characteristics of the 3.3-kV/750-A SiC-MOSFET implemented in the model of the resonant isolated dc/dc converter.

Regarding the calculation of the transformer losses, the PLECS model used for the simulations is based only on constant values of series resistance and core loss equivalent resistance (see Table I).

TABLE III

CHARACTERISTICS OF THE 3.3-kV/750-A SiC-MOSFET HBM AND CALCULATION OF LOSSES

MOSFET	Diode
Conduction losses equation:	
$P_{\text{cond MOS}} = R_{\text{ds ON}}(T_j) \cdot I_{\text{MOS RMS}}^2$	$P_{\text{cond D}} = R_d(T_j) \cdot I_{\text{D RMS}}^2 + V_0(T_j) \cdot I_{\text{D AVG}}$
Static characteristics @ $T_{j\max} = 175^\circ\text{C}$:	
$R_{\text{ds ON}} = 5.2 \text{ m}\Omega$	$R_d = 3.42 \text{ m}\Omega ; V_0 = 1.25 \text{ V}$
Switching energy losses equation (polynomial model):	
$E_{\text{on}}(V_{\text{ds}}, T_j) = a_{\text{on}}(V_{\text{ds}}, T_j) \cdot i_{\text{on}}^2 + b_{\text{on}}(V_{\text{ds}}, T_j) \cdot i_{\text{on}} + c_{\text{on}}(V_{\text{ds}}, T_j)$	$E_{\text{rec}}(V_{\text{ds}}, T_j) = a_{\text{rec}}(V_{\text{ds}}, T_j) \cdot i_{\text{rec}}^2 + b_{\text{rec}}(V_{\text{ds}}, T_j) \cdot i_{\text{rec}} + c_{\text{rec}}(V_{\text{ds}}, T_j)$
$E_{\text{off}}(V_{\text{ds}}, T_j) = a_{\text{off}}(V_{\text{ds}}, T_j) \cdot i_{\text{off}}^2 + b_{\text{off}}(V_{\text{ds}}, T_j) \cdot i_{\text{off}} + c_{\text{off}}(V_{\text{ds}}, T_j)$	
Dynamic characteristics @ $V_{\text{ds}} = 1.8 \text{ kV}$; $T_{j\max} = 175^\circ\text{C}$:	
$a_{\text{on}} = 3.22 \times 10^{-7} ; b_{\text{on}} = 5.51 \times 10^{-4} ; c_{\text{on}} = 1.14 \times 10^{-2}$	$a_{\text{rec}} = -1.77 \times 10^{-9} ; b_{\text{rec}} = 1.95 \times 10^{-5} ; c_{\text{rec}} = 1.76 \times 10^{-2}$
$a_{\text{off}} = 2.44 \times 10^2 ; b_{\text{off}} = 2.40 \times 10^{-4} ; c_{\text{off}} = -1.50 \times 10^{-2}$	
Losses equation:	
$P_{\text{MOS}} = P_{\text{cond MOS}} + f_{\text{sw}} \cdot (E_{\text{on}} + E_{\text{off}})$	$P_D = P_{\text{cond D}} + f_{\text{sw}} \cdot E_{\text{rec}}$
Thermal characteristics (1/2 module):	
$R_{\text{th(j-q)max}} = 32 \text{ K/kW}$	$R_{\text{th(j-q)max}} = 54.5 \text{ K/kW}$
Thermal resistance Case to Heat sink:	
$R_{\text{th(c-s)max}} = 22.5 \text{ K/kW} @ \lambda_{\text{grease}} = 1 \text{ W/m}\cdot\text{K} ; D_{\text{(c-s)}} = 100 \mu\text{m}$	
Thermal resistance Heat sink to Ambiant ($T_{\text{amb}} = 40^\circ\text{C}$):	
$R_{\text{th(h-a)max}} = 10 \text{ K/kW}$ (water cold plate at 5 litres/min)	

TABLE IV

SIMULATION RESULTS' COMPARISON OF THREE OPERATING MODES OF THE RESONANT ISOLATED DC-DC CONVERTER $V_{\text{in}} = 1800 \text{ V}$, $f_{\text{sw}} = 15 \text{ kHz}$, TURNS RATIO 1:1, AND $I_{\text{out}} = 170 \text{ A}$

	R-DAB	R-SAB CCM	R-SAB DCM
AC RMS current (I_{ac})	198 A _{rms}	188 A _{rms}	215 A _{rms}
Series capacitor RMS voltage (V_{Cr})	1156 V _{rms}	203.9 V _{rms}	738.8 V _{rms}
Series capacitor reactive power (Q_{Cr})	226.7 kVAR	37.6 kVAR	154.3 kVAR
MFT apparent power (S_{rms})	478.6 kVA	355.1 kVA	374.2 kVA
Output voltage (V_{out})	1800 V	1709 V	1794 V
Output power (P_{out})	306.0 kW	290.5 kW	305.0 kW
Input power (P_{in})	307.9 kW	292.4 kW	307.2 kW
Primary side H-Bridge losses	1471 W	2172 W	269 W
Secondary side H-Bridge losses	1553 W	499 W	551 W
MFT losses	1097 W	990 W	1139 W
Total losses	4121 W	3661 W	1959 W
Power efficiency (η)	98.67%	98.76%	99.36%

D. Simulation Results and Choice of Operating Mode of the Resonant Isolated DC/DC Converters

The simulation results presented in Table IV were obtained from the electric-thermal model presented previously.

The simulation waveforms, for the operating points corresponding to Table IV, are presented in Fig. 7.

TABLE V

MFT PROTOTYPE SPECIFICATIONS

Input voltage	$V_{\text{in}} = 1800 \text{ V}$
Turns ratio	1 : 1
Nominal current	$I_{\text{rms}} = 230 \text{ A}$
Apparent power	$S_{\text{rms}} = 400 \text{ kVA}$
Isolation level	$V_{\text{iso}} = 20 \text{ kV}$ (tested @ 5 kV)
Total weight	160 kg
Volume	45 litres
Cooling fluid	water (flow rate of 5 litres/min)

TABLE VI

R-SAB DCM PROTOTYPE SPECIFICATIONS

Input voltage	$V_{\text{in}} = 1800 \text{ V}$
Converter nominal output current	$I_{\text{out}} = 170 \text{ A}$
Converter nominal output power	$P_{\text{out}} \approx 300 \text{ kW}$
SiC-MOSFET HBM	Mitsubishi 3.3 kV / 750 A
Si-Diode HBM	ABB 3.3 kV / 500 A
Gate-Driver [35] (with optical interface)	$V_{\text{gs}} = -5 / +17 \text{ V}$
Switching frequency	$f_{\text{sw}} = 15 \text{ kHz}$
Dead-time on voltage source inverter	5 μs
Semiconductors heatsinks	water cold plates from Mersen
Water flow rate	$Q_v = [1 - 5] \text{ litres/min}$
Input/output Capacitors	Electronics Concepts - LH3 series
Resonant Capacitor	Illinois Capacitor - HC5 series
Sensors	LEM series LV and DV
Control system	Imperix BoomBox with optical interface

Fig. 8 shows the losses and the efficiency as a function of the output current for these three operating modes. Due to the phase shift control, the R-DAB operation involves more reactive power in the ac stage and, thus, requires a transformer with a higher power rating. In the considered application, the output power of the converter depends on the current drawn by the traction inverters of the locomotives. Thus, R-DAB operation with the control of power flow by phase shifting is not necessary. Regarding the sizing of the resonance capacitor, the operation in R-SAB CCM is more attractive. Nevertheless, for railway network operators, the cost of ownership of a converter over a long operating period (30–40 years) is essential, and the losses have to be seriously considered. As a result, the DCM operating mode of the R-SAB was selected as it shows the highest efficiency.

IV. EXPERIMENTAL TESTS AND RESULTS

A. Design of the 300-kW-15-kHz Resonant Single Active Bridge

Tables V and VI, respectively, summarize the specifications of the MFT and the specifications of the R-SAB prototype. At these levels of ac current and operating frequency,

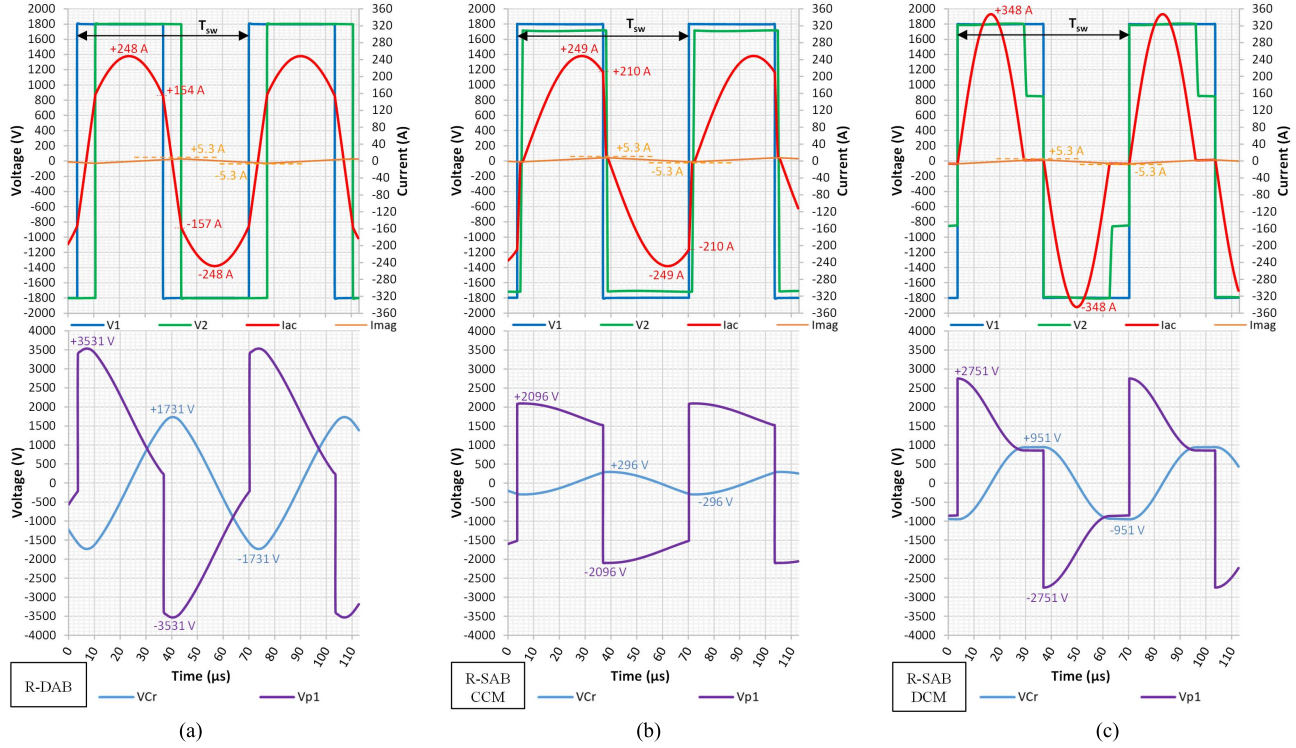


Fig. 7. Isolated resonant dc/dc converter—simulation waveforms with PLECS software for the three operating modes. (a) R-DAB. (b) R-SAB CCM. (c) R-SAB DCM.

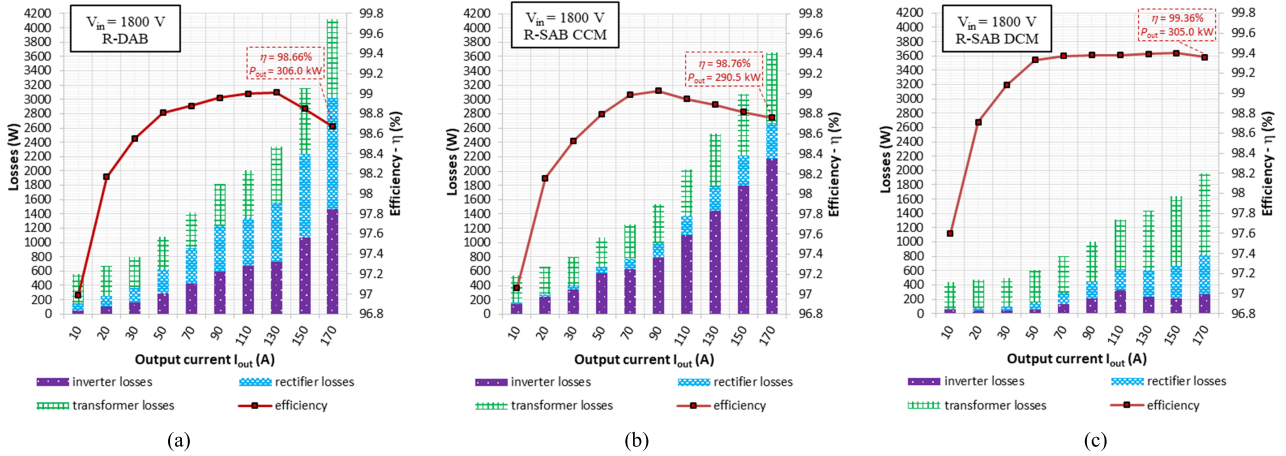


Fig. 8. Isolated resonant dc/dc converter—comparison of the different losses and efficiency of the three operating modes. Calculation results (PLECS electric–thermal model). (a) R-DAB. (b) R-SAB CCM. (c) R-SAB DCM.

the choice of the resonant capacitor is a key point. In our case, a metalized polypropylene dielectric technology, specially designed for very high reactive power, is chosen. Capacitors from Illinois Capacitor Inc. [48], designed to operate up to a frequency of 100 kHz, were associated in series/parallel to obtain 3 μ F. As shown in Fig. 9(a), their geometrical design with a large connection surface allows a direct mounting on busbars, improves the heat transfer, and leads to a very low stray inductance (less than 3 nH). Thus, for the rating corresponding to the R-SAB DCM operation (see Table II), the total volume of capacitors is about 0.36 L. For the nominal operating point of the converter, the voltage at these terminals does not exceed 755 V_{rms} for an ac current of 223 A_{rms}.

The losses are less than 30 W and can be considered negligible compared with the other losses in the converter.

Initially, for cost reasons, silicon diodes were used in the output rectifier. The SiC-MOSFET modules were introduced in the output stage once the correct operation of the converter was confirmed up to its nominal rating. For the final tests, the same SiC modules were used both on the inverter and the rectifier.

Thus, the Schottky SiC-diodes realize a simple rectifier-bridge when the MOSFETs are turned off.

Nevertheless, it is also possible to achieve synchronous rectification. The SiC-MOSFETs are then used to conduct a reverse current and, thus, reduce the conduction losses

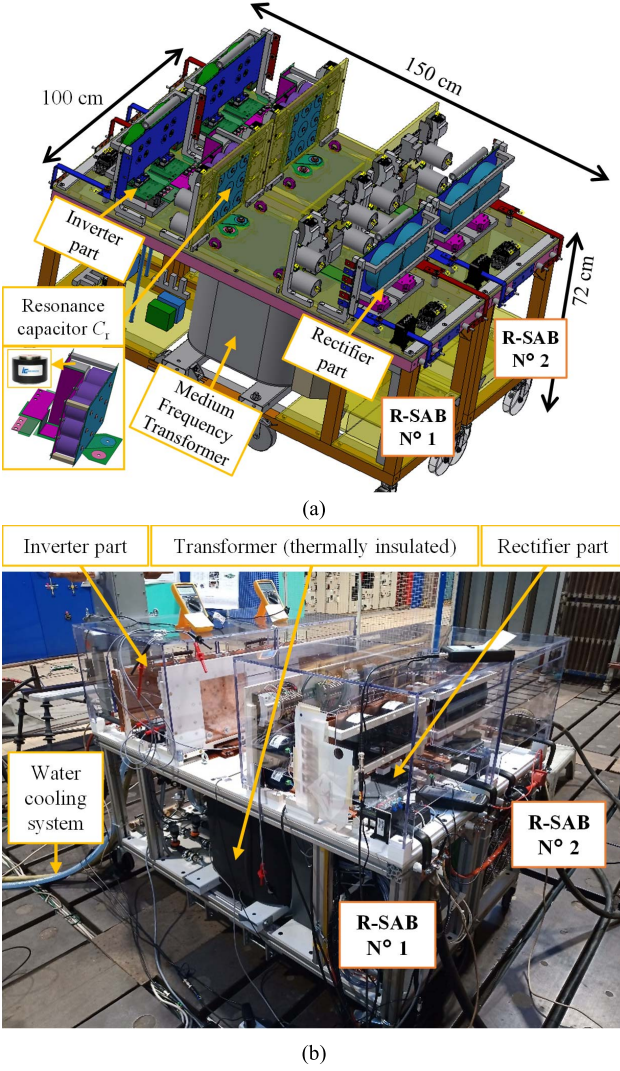


Fig. 9. ISOP association of two R-SABs prototypes. (a) 3-D Mechanical design. (b) Picture of the prototypes under test.

while better distributing the losses in the module. As a result, a comparison between a solution based on Si-diodes (ABB 3.3 kV/500 A) and a solution based on SiC-diodes (Mitsubishi 3.3 kV/750 A) is presented in the following.

In order to validate the ISOP association of R-SABs with a natural balancing of currents and voltages between the converters, two identical prototypes were built. This configuration realizes a 3-kV/1.5-kV isolated power converter with a maximum input voltage of 3600 V and a doubled output current. Fig. 9 shows the 3-D mechanical design and a picture of two R-SABs prototypes in the ISOP association.

B. Characterization of One Converter Using the Opposition Method

In order to accurately characterize R-SAB, the opposition method is used [35], [49], [50]. In our case study, the R-SAB structure includes a transformer with a voltage ratio equal to 1. Consequently, the direct connection between the input and the output is possible because the two sides of the converter are identical, and they share a common transformer with a unity transformation ratio allowing the output to be connected to

the input. There is, therefore, no need for a second converter to implement the opposition method. Thus, Fig. 10 shows the resulting circuit implemented. The voltage source (V_{dc}) imposes the voltage (V_{in}) on the input dc bus, while the current source regulates the output current (I_{out}) flowing in the converter. In addition, a filter inductor (L_{io}) of 230 μ H and an input inductor (L_{in}) of 1 mH are added to avoid the circulation of high-frequency currents in the power supplies. Otherwise, a diode is added at the input to protect the voltage generator from any reverse currents. Thus, the two power supplies provide only the losses of the converter. The role of the voltage source is to supply the losses, mainly linked to the magnetization of the transformer, which, in practice, corresponds to a current of a few amps. The current source supplies all the other losses (conduction and switching) of the R-SAB structure. It imposes the output current I_{out} with a very low voltage (a few tens of volts) corresponding to the voltage drop of the converter (ΔV).

The test bench measures converter losses both electrically (input power measurement) and thermally (output coolant measurement) [35], [49]. As shown in Fig. 10, three water-cooling circuits are used in parallel to estimate the losses by calorimetry. This method consists of measuring the cooling-water flow and the inlet and outlet temperatures of each of these three circuits. In order to achieve accurate measurements, convected heat dissipation is limited by the use of specific insulating foams (visible in black around the MFT in Fig. 9). The electrical method is based on the measurements of currents I_{in} and I_{out} and voltages V_{out} and V_{in} . From these measurements, the R-SAB total losses by the electrical method are calculated according to the following equation:

$$P_{\text{electrical method}} = (V_{in} \times I_{in}) + ((V_{in} - V_{out}) \times I_{out}). \quad (6)$$

For the calorimetric method, (7) and (8) give the losses as a function of the thermodynamic parameters of R-SAB total losses and the losses in the inverter, the transformer, and the rectifier

$$P_{\text{calorimetric method}} = P_{\text{inv}} + P_{\text{transfo}} + P_{\text{rect}} \quad (7)$$

$$\begin{cases} P_{\text{inv}} = \rho \times C_p \times Q_{\text{inv}} \times (T_{out_{\text{inv}}} - T_{in_{\text{inv}}}) \\ P_{\text{transfo}} = \rho \times C_p \times Q_{\text{tra}} \times (T_{out_{\text{tra}}} - T_{in_{\text{tra}}}) \\ P_{\text{rect}} = \rho \times C_p \times Q_{\text{rect}} \times (T_{out_{\text{rect}}} - T_{in_{\text{rect}}}) \end{cases} \quad (8)$$

where $(T_{out_x} - T_{in_x}) = \Delta T$ is the temperature difference of cooling water between the inlet and outlet of the heat sink [$^{\circ}\text{K}$]; ρ is the density of the coolant [kg/m^3]; C_p is the specific heat of water [$\text{J}/(\text{kg} \cdot \text{K})$]; and Q_x is the flow rate of cooling water [m^3/s].

After initial calibration and testing of both methods, as mentioned earlier, the first results were obtained with Si-diode modules in the output rectifier, and in the second round of measurements, SiC modules were mounted in the output rectifier.

C. Characterization Results by Opposition Method

The output characteristics of the elementary isolated dc/dc converters are presented in Fig. 11 for the different solutions proposed for the output rectifier. Theoretically, in DCM

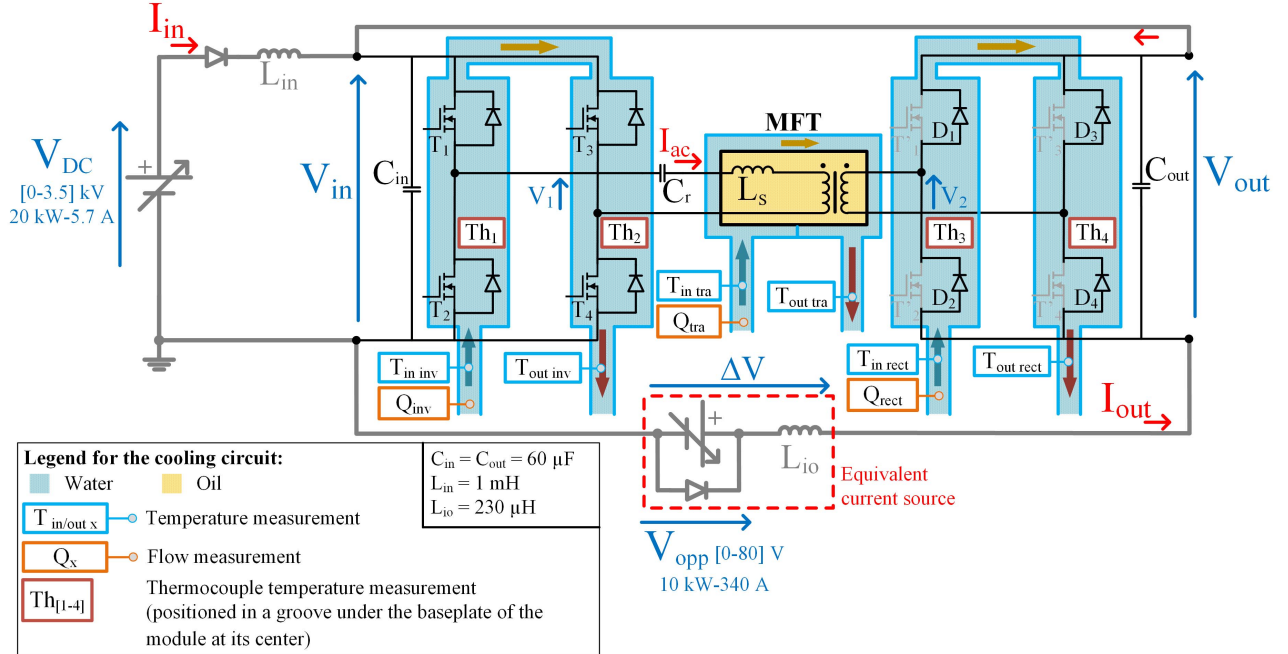


Fig. 10. Schematic of the circuit used for the experimental tests by the opposition method.

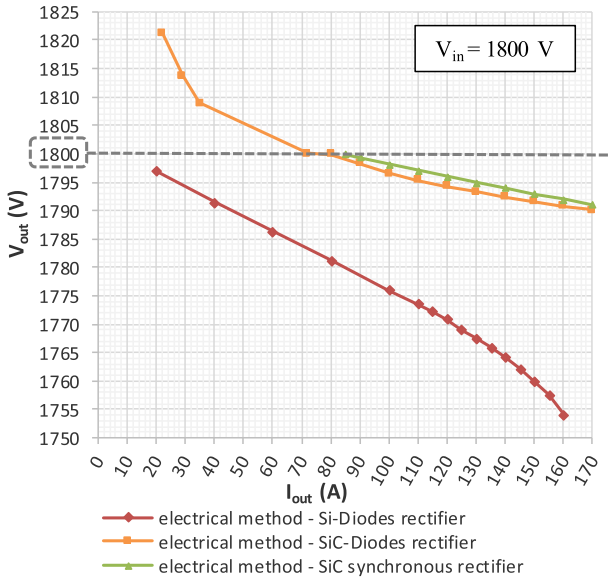


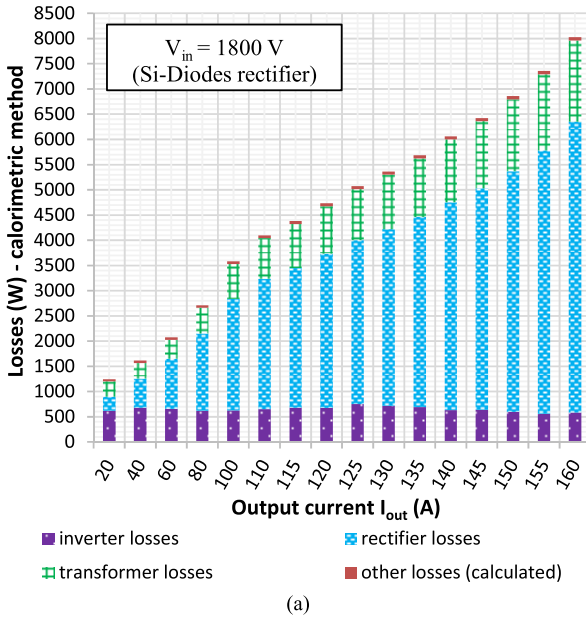
Fig. 11. Comparison of the R-SAB output characteristics for the case with the Si-diodes and the case with the SiC-diodes (with and without synchronous rectifier).

operation, the output characteristic corresponds to that of a voltage source with an internal voltage drop proportional to the output current. However, the experimental curves show that this is more complex. Indeed, the parasitic capacitances of the assembly strongly influence these characteristics and lead to a voltage step-up operation at a low output current. Indeed, for an input voltage of 1.8 kV and at no-load operation, the output voltage V_{out} rises to 2.2 kV. This phenomenon is more sensitive when SiC-MOSFET modules are used in the output rectifier. The output voltage V_{out} becomes lower than the input

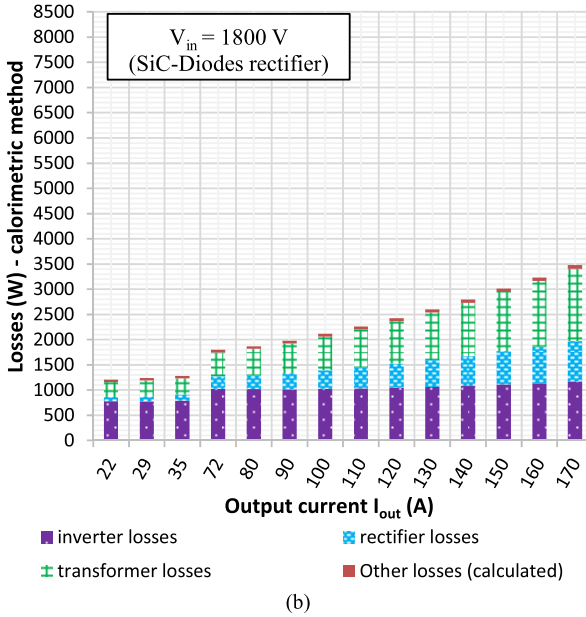
voltage V_{in} from an output-current level of about 20 A in the case of Si-diodes and 70 A in the case of SiC-modules. This is explained by the fact that Si-diode modules show lower parasitic capacitances than SiC-MOSFET modules. For the opposition test method, this voltage boost required the insertion of a resistor in series with the current source in order to keep the controllability of the operating points. However, this low-current voltage boost is not problematic for the final application since the overvoltage is, in practice, minimized by the fact that the converters must always supply the minimal load presented by the auxiliaries.

Fig. 12 shows different losses obtained with the calorimetric method, in the cases with Si-diodes [see Fig. 12(a)] and SiC-diodes [see Fig. 12(b)]. These tests required a fairly long time of more than 3 h at each operating point in order to obtain a correct calorimetric measurement for the transformer. Indeed, the transformer contains oil, and this, combined with the water circuit located on its outside, results in a thermal time constant of approximately 1 h. On the other hand, this allowed the R-SAB to be tested over many hours of operation.

Despite the low di/dt operation of the resonant circuit, these tests show that the recovery losses on the 3.3-kV Si-diodes, at 15 kHz, are very high. The thermal limit of these diodes is reached for an output current of 160 A, which is slightly lower than the specified nominal value. On the other hand, as SiC-diodes have no reverse-recovery current, the losses are very low, and the output current can go up to the nominal value of 170 A. However, the use of SiC-MOSFET modules in the output rectifier leads to a slight increase of the voltage-source inverter losses. As explained previously, the SiC-MOSFET modules introduce parasitic capacitances greater than those of the Si-diode modules. Thus, on the voltage-source inverter, during the dead time, the evolution of the



(a)



(b)

Fig. 12. Comparison of the different losses of the R-SAB with calorimetric measurements. (a) Solution with Si-diode in the output rectifier. (b) Solution with SiC-diode in the output rectifier.

voltage across the MOSFETs is slowed down. As a result, the MOSFETs are turned on at a higher voltage level, which slightly increases the switching losses. For the operating point $V_{in} = 1800$ V and $I_{out} = 150$ A, Fig. 13 shows a superposition of the measured switching waveforms for MOSFETs (V_{ds} , I_{ds} , and V_{gs}) of the voltage-source inverter in the cases of Si-diodes [see Fig. 13(a)] and SiC-diodes [see Fig. 13(b)] in the output rectifier.

The total converter losses are presented in Fig. 14, for the thermal and electrical measurement methods. Beyond the good correlation of the two methods, these measurements highlight the importance of using SiC-diodes in the output rectifier. For example, the operating point with an output current of 160 A leads to a reduction of the total losses of approximately 56%.

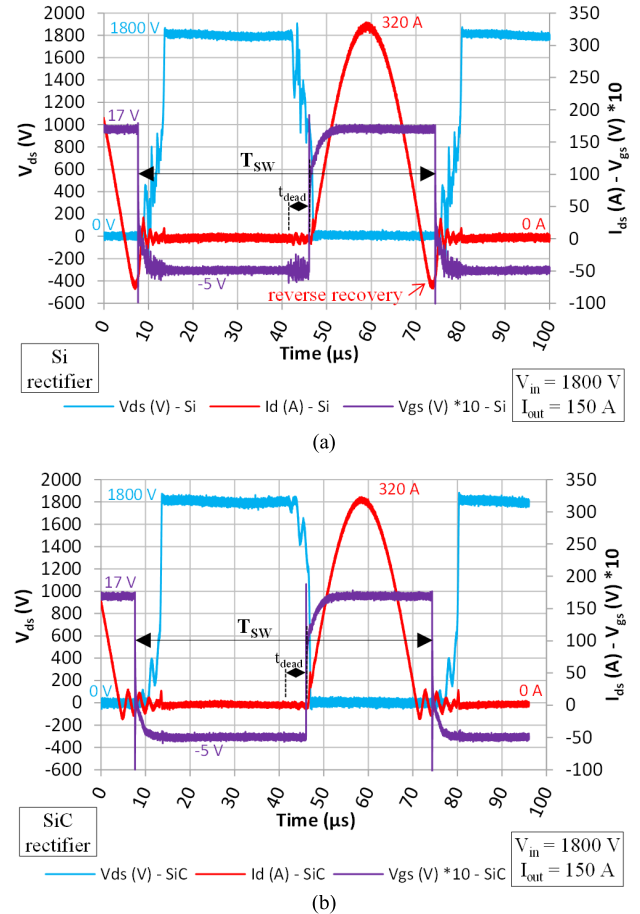


Fig. 13. Comparison by the overlay of experimental waveforms of the switching of one of the MOSFETs of the inverter with the rectifier equipped with (a) Si-diode and (b) SiC-diode.

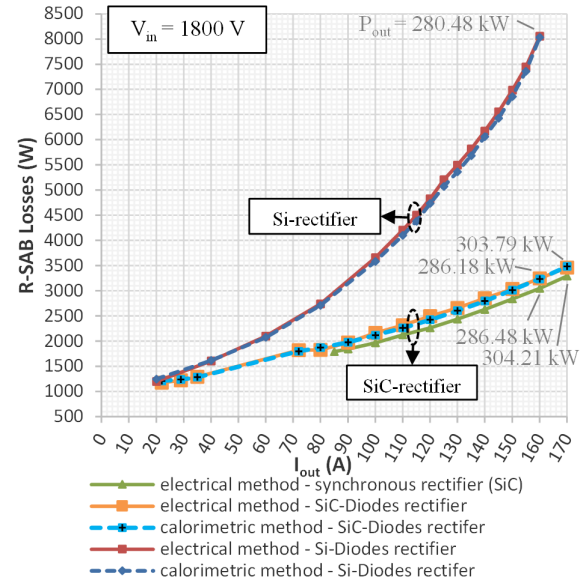


Fig. 14. Comparison of the total losses of the R-SAB for the case with the Si-diodes and the case with the SiC-diodes (with and without synchronous rectifier).

Fig. 15 shows the R-SAB efficiency as a function of output current I_{out} . For the solution with a rectifier based on Si-diodes, maximum efficiency of 98.1% is reached at an

TABLE VII

RESULTS OF EXPERIMENTAL MEASUREMENTS WITH TWO R-SABs IN ISOP ASSOCIATION, FOR SEVERAL OUTPUT CURRENT VALUES (I_{out}), BY CHANGING THE VALUE OF THE LOAD RESISTANCE (R_{load})

$R_{\text{load}} (\Omega)$	1100 (K_{load} open)	23	16	13	10	8	7
V_{in} (V)	3589.17	3594.55	3601.53	3599.92	3598.76	3597.13	3598.67
$V_{\text{in}1}$ (V)	1796.63	1797.55	1801.01	1800.17	1799.63	1798.71	1799.24
$V_{\text{in}2}$ (V)	1792.54	1797	1800.51	1799.75	1799.12	1798.41	1799.43
relative error (%) between $V_{\text{in}1}$ and $V_{\text{in}2}$	0.23	0.03	0.03	0.02	0.03	0.02	0.01
$I_{\text{ac}1}$ (A) - RMS		48.1	67.1	75.6	106.3	133.3	149.1
$I_{\text{ac}2}$ (A) - RMS		47.6	66.4	74.8	105.4	130.9	146.1
relative error (%) between $I_{\text{ac}1}$ and $I_{\text{ac}2}$		1.05	1.05	1.07	0.85	1.83	2.05
V_{out} (V)	1814.51	1789.79	1789.49	1786.2	1780.64	1774.8	1772.11
I_{in} (A)	0.96	36.26	50.84	62.64	81.16	100.66	114.51
I_{out} (A)	1.48	72.56	102.19	126.22	164	203.75	231.97
$\Delta V = (V_{\text{in}} - V_{\text{out}})$ (V)	-19.93	7.49	11.27	13.75	18.74	23.77	27.22
$P_{\text{out}} = V_{\text{out}} * I_{\text{out}}$ (kW)	2.68	129.86	182.86	225.45	292.02	361.62	411.08
% of $P_{\text{out MAX}}$ (2*280.48 kW = 560.96 kW see Fig. 14)	0.48	23.15	32.60	40.19	52.06	64.46	73.28

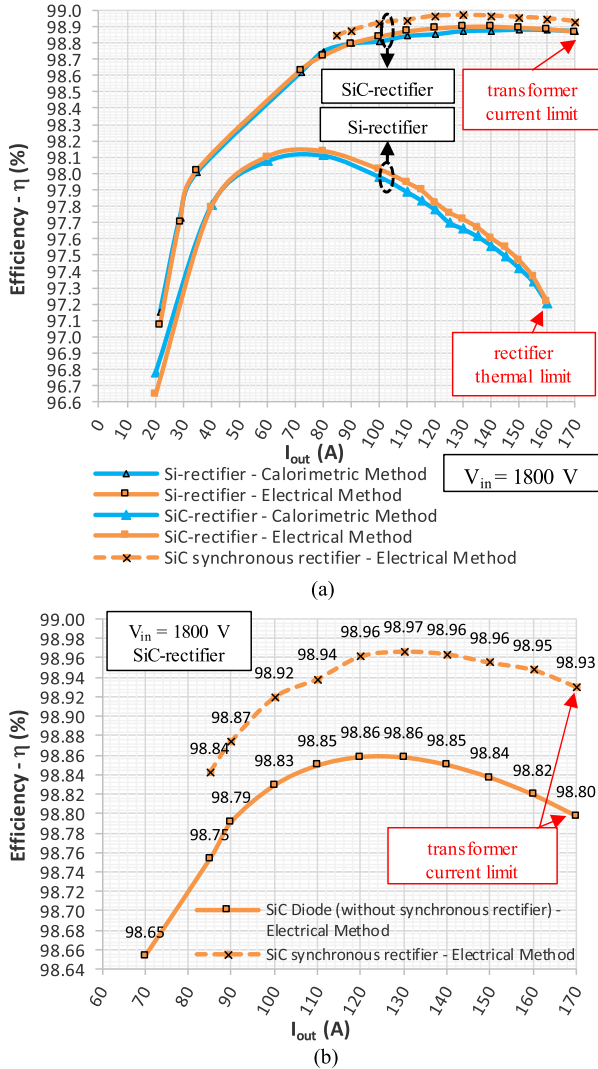


Fig. 15. R-SAB efficiencies using Si-diodes compared with SiC-diodes (with and without synchronous rectifier). (a) Full current range. (b) Zoom on the SiC high-current range with and without SiC synchronous rectifier.

output current of 70 A. Beyond this output current value, the efficiency decreases to 97.2% at $I_{\text{out}} = 160$ A due to the recovery losses. For the SiC-diode solution, the efficiency reaches

a maximum of 98.86% at 120 A and then decreases slightly to 98.80% at $I_{\text{out}} = 170$ A. Finally, as shown in Fig. 15(b), the synchronous rectifier operation makes it possible to further increase efficiency. It is 98.93% instead of 98.80% for the operating point $V_{\text{in}} = 1800$ V and $I_{\text{out}} = 170$ A.

For this type of SiC-MOSFET module, including SiC-Schottky diodes, the gain in efficiency is not significant compared with the changes that must be made on the converter (additional ac sensor and control board). The synchronous-rectifier operation has undoubtedly its value for modules using only SiC-MOSFET dies because it avoids the conduction of the body diodes.

Otherwise, if the power reversibility of the isolated dc/dc converter is not required, it is possible to implement, in the output rectifier, power modules using only SiC-Schottky diodes, which is the simpler solution allowing lower cost.

Overall, these results show that, at the considered experimental power level, tests are essential. The comparison between Figs. 8(c) and 12(b) shows that the loss measurements performed during the tests are quite different from the preliminary calculations based on simulations: @ $I_{\text{out}} = 170$ A, the measured total losses are 3.4 kW, while, in simulations, the calculations' results give 1.96 kW. In simulations, the losses in the SiC power modules and the transformers are both underestimated. This can be explained by the fact that the behavior of the semiconductor devices in the ZVS or ZCS mode is completely different than in hard-switching. The MOSFET modules are initially developed for motor-driven voltage-source inverters, and the manufacturer gives only switching energy curves for this application. The use of these energy curves in thermal models is, therefore, inaccurate. Furthermore, the transformer electrical model used in simulations does not take into account the effect of harmonics on core and winding losses.

D. Test Results With Two R-SABs in ISOP Association

As presented in Fig. 5, the final application will include an ISOP association of six submodules to step down the voltage from 9 to 1.5 kV. Considering available experimental means and for cost reasons, it was decided to test the association

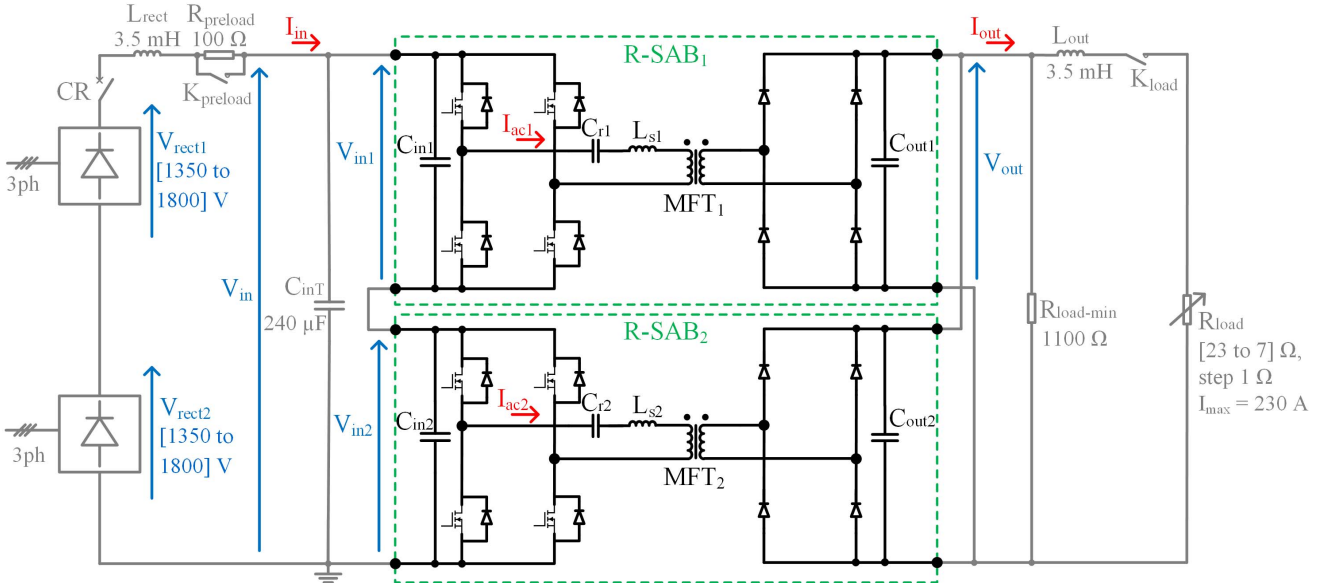


Fig. 16. Schematic of the circuit used for the experimental tests with two R-SABs in the ISOP association at the French Railways test platform.

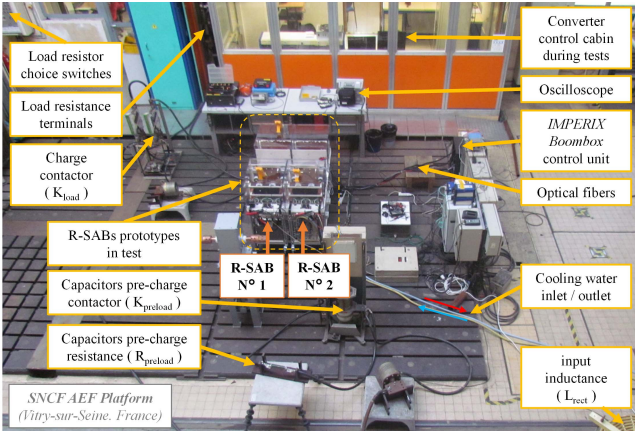


Fig. 17. Overview of the test bench with two R-SABs in the ISOP association at the French Railways test platform.

of only two R-SABs using Si-diode modules. This association allows us to obtain a 3.6-/1.8-kV dc–dc converter with a power rating of 600 kW. The aim of these tests was to verify the natural current and voltage sharing between the elementary converters in the ISOP association. As shown in Fig. 9, the busbars of the converters were designed to facilitate the series connection of the inputs and the parallel connections of the outputs. Due to the experience accumulated on previous prototypes [35], [49], the busbars were initially designed to achieve an association of six elementary R-SABs without too much technical difficulty (connections, conductive sections, and insulations).

Fig. 16 shows the diagram of the circuit used for the tests. Fig. 17 shows an overview of the two isolated dc/dc converters installed on the SNCF testbed in Vitry, France. Two conventional six-pulse rectifiers are associated in series in order to reach the 3600 V required for the tests. A 400-kW resistive load bank (R_{load}), whose values are adjustable from 7 to 23 Ω in steps of 1 Ω , is used. In addition, a minimum load ($R_{load-min}$) of 1100 Ω is placed at the output of the converters,

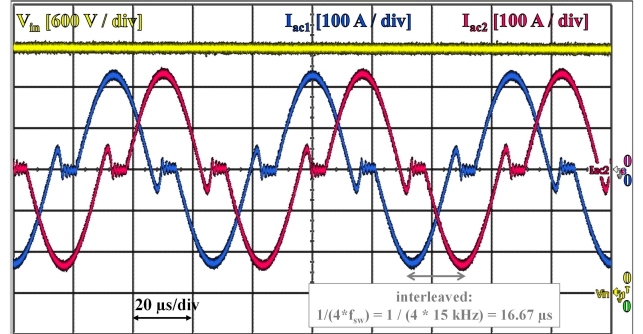


Fig. 18. Experimental waveforms of the interleaved current at the input of the two medium-frequency transformers for $V_{in} = 3600$ V and $R_{load} = 7 \Omega$ ($I_{out} = 232$ A).

in order to limit output voltage V_{out} at 1825 V when the input voltage V_{in} is set at 3600 V and the high-power load bank (R_{load}) is disconnected.

In order to get a high-frequency ripple at four times the switching frequency (60 kHz), on the output voltage V_{out} , the control patterns of the two R-SABs are interleaved by a quarter of the switching period, as shown in Fig. 18. Moreover, due to the current and voltage sensors implemented on the test bench, the control system is able to turn off the MOSFETs and to open CR in the case of current-overload, voltage-imbalance between the two R-SABs or fault-detection in the gate drivers [35].

The converter is powered up by closing the CR. The resistor, $R_{preload}$, allows the charging of all the capacitors in the circuit. Once the voltage has been established on the two converters, the precharge resistor is short-circuited with the contactor $K_{preload}$, and it is then possible to connect the resistive load bank by closing the contactor K_{load} . The load bank is equipped with contactors that change the load resistance and adjust the output current I_{out} .

Table VII shows the electrical measurements for an input voltage at 3600 V and for several load-resistance values.

The natural balancing of input voltages and output currents between the two converters is experimentally confirmed. It should be noted that, the load-power being limited to 411 kW, it was not possible, during the tests, to reach the maximum output power of 600 kW for the two-converter association.

V. CONCLUSION

Taking into account the characteristics of the power modules (3.3 kV/750 A), the power rating of the elementary isolated dc–dc converter has been set to 300 kW with a switching frequency at 15 kHz. The experimental results presented in this article have demonstrated the short-term feasibility of an industrial solution since 3.3-kV SiC MOSFET modules are now in production and MFT technology is the state of the art for traction-transformer manufacturers. First, a preliminary study based on the electrothermal simulation on the PLECS software allowed to select the operating mode of the resonant isolated dc/dc converter and made it possible to size the test bench but also quantify the losses and the efficiency. Second, the efficiency was accurately assessed using electrical and thermal loss measurements on the converter tested with an opposition method. Initially implemented for the first tests, the solution using Si-diodes in the output rectifier is not attractive (the recovery currents lead to high turn-off losses). In fact, the only acceptable solution is the use of SiC-Schottky diodes allowing the nominal current of the transformer to be reached ($I_{ac-\text{rms}} = 223$ A) at an efficiency of 98.80% for an output power of 300 kW. In order to take advantage of the SiC-MOSFETs present in the power modules used in the output rectifier, a synchronous-rectifier operation has also been tested. It was then possible to reach an efficiency of 98.93% for an output power of 300 kW. This is quite remarkable for an isolated dc–dc converter operating under 1.8 kV with a switching frequency of 15 kHz. Finally, two elementary dc–dc converters were associated with ISOP configuration to form a 3.6-/1.8-kV PET. These tests, performed on an SNCF testbed, required the series connection of two six-pulse rectifiers and the use of a resistive high-power load bank. The natural power-sharing between the two converters has been demonstrated. The results presented in this article are promising, and they encourage the SNCF to continue with the MVdc electrification project. A very efficient and compact PET, based on the association of isolated elementary dc–dc converters, is entirely feasible. The next step is to associate, in the ISOP configuration, six isolated elementary dc–dc converters to achieve a 9-/1.5-kV PET with a power rating of 1.8 MW.

ACKNOWLEDGMENT

The authors would like to thank the staff of the AEF test site in Vitry-sur-Seine, France, and in particular, Mr. Aboudrar Saïd and his team.

REFERENCES

- [1] *Railway Applications—Power Supply and Rolling Stock—Technical Criteria for the Coordination Between Power Supply (Substation) and Rolling Stock to Achieve Interoperability*, document EN 50388, Apr. 2012.
- [2] *Railway Applications—Supply Voltages of Traction Systems*, document IEC 60850, 4th ed., 2014.
- [3] A. Steimel, “Under Europe’s incompatible catenary voltages a review of multi-system traction technology,” in *Proc. Electr. Syst. Aircr., Railway Ship Propuls.*, Bologna, Italy, Oct. 2012, pp. 1–8.
- [4] S. M. M. Gazarfudi, A. T. Langerud, E. F. Fuchs, and K. Al-Haddad, “Power quality issues in railway electrification: A comprehensive perspective,” *IEEE Trans. Ind. Electron.*, vol. 62, no. 5, pp. 3081–3090, May 2015.
- [5] D. Frugier and P. Ladoux, “Voltage disturbances on 25kV-50 Hz railway lines—modelling method and analysis,” in *Proc. Int. Symp. Power Electron., Electr. Drives, Autom. Motion (SPEEDAM)*, Pisa, Italy, Jun. 2010, pp. 1080–1085.
- [6] N. Golovanov, G. C. Lazarou, M. Roscia, and D. Zaninelli, “Voltage unbalance vulnerability areas in power systems supplying high speed railway,” in *Proc. IEEE Power Eng. Soc. Gen. Meeting*, San Francisco, CA, USA, vol. 3, 2005, p. 2509.
- [7] T. Lagier, P. Ladoux, and P. Dworakowski, “Potential of silicon carbide MOSFETs in the DC/DC converters for future HVDC offshore wind farms,” *High Voltage*, vol. 2, no. 4, pp. 233–243, Dec. 2017.
- [8] A. Verdicchio, P. Ladoux, H. Caron, and C. Courtois, “New medium-voltage DC railway electrification system,” *IEEE Trans. Transport. Electricif.*, vol. 4, no. 2, pp. 591–604, Jun. 2018.
- [9] U. Javaid, D. Dujic, and W. van der Merwe, “MVDC marine electrical distribution: Are we ready?” in *Proc. 41st Annu. Conf. IEEE Ind. Electron. Soc. (IECON)*, Yokohama, Japan, Nov. 2015, pp. 823–828.
- [10] C. Meyer, M. Kowal, and R. W. De Doncker, “Circuit breaker concepts for future high-power DC-applications,” in *Proc. 14th IAS Annu. Meeting. Conf. Rec. Ind. Appl. Conf.*, vol. 2, 2005, pp. 860–866.
- [11] T. Augustin, M. B. Garcia, J. Magnusson, H.-P. Nee, and M. Parekh, “System design of fast actuator for vacuum interrupter in DC applications,” in *Proc. 28th Int. Symp. Discharges Electr. Insul. Vac. (ISDEIV)*, Greifswald, Germany, Sep. 2018, pp. 527–530.
- [12] X. Song, C. Peng, and A. Q. Huang, “A medium-voltage hybrid DC circuit breaker, Part I: Solid-state main breaker based on 15 kV SiC emitter turn-OFF thyristor,” *IEEE J. Emerg. Sel. Topics Power Electron.*, vol. 5, no. 1, pp. 278–288, Mar. 2017.
- [13] N. Hatti, K. Hasegawa, and H. Akagi, “A 6.6-kV transformerless motor drive using a five-level diode-clamped PWM inverter for energy savings of pumps and blowers,” *IEEE Trans. Power Electron.*, vol. 24, no. 3, pp. 796–803, Mar. 2009.
- [14] A. Verdicchio, P. Ladoux, H. Caron, and S. Sanchez, “Future DC railway electrification system-go for 9 kV,” in *Proc. IEEE Int. Conf. Electr. Syst. Aircr., Railway, Ship Propuls. Road Vehicles Int. Transp. Electricif. Conf. (ESARS-ITEC)*, Nottingham, U.K., Nov. 2018, pp. 1–5.
- [15] J. Feng, W. Q. Chu, Z. Zhang, and Z. Q. Zhu, “Power electronic transformer-based railway traction systems: Challenges and opportunities,” *IEEE J. Emerg. Sel. Topics Power Electron.*, vol. 5, no. 3, pp. 1237–1253, Sep. 2017.
- [16] D. Ronanki, S. A. Singh, and S. S. Williamson, “Comprehensive topological overview of rolling stock architectures and recent trends in electric railway traction systems,” *IEEE Trans. Transport. Electricif.*, vol. 3, no. 3, pp. 724–738, Sep. 2017.
- [17] A. Kadavelugu *et al.*, “Medium voltage power converter design and demonstration using 15 kV SiC N-IGBTs,” in *Proc. IEEE Appl. Power Electron. Conf. Exposit. (APEC)*, Charlotte, NC, USA, Mar. 2015, pp. 1396–1403.
- [18] F. Morel *et al.*, “Power electronic traction transformers in 25 kV/50 Hz systems: Optimisation of DC/DC isolated converters with 3.3 kV SiC MOSFETs,” in *Proc. PCIM Eur.*, Nuremberg, Germany, 2019, pp. 553–560.
- [19] H. Hayashiya *et al.*, “Review of regenerative energy utilization in traction power supply system in Japan: Applications of energy storage systems in D.C. traction power supply system,” in *Proc. 43rd Annu. Conf. IEEE Ind. Electron. Soc. (IECON)*, Oct. 2017, pp. 3918–3923.
- [20] European Commission—CORDIS UE Research Results—Future Unified DC Railway Electrification System. Accessed: Mar. 2020. [Online]. Available: <https://cordis.europa.eu/project/id/881772/>
- [21] Roll2Rail. Deliverables: D 1.2 New Generation Power Semiconductor—R2R-T1.I-D-BTS-030-07. Accessed: Mar. 2020. [Online]. Available: <http://www.roll2rail.eu/>
- [22] R. Schnell, S. Hartmann, D. Truessel, F. Fischer, A. Baschnagel, and M. Rahimo, “LinPak, a new low inductive phase-leg IGBT module with easy paralleling for high power density converter designs,” in *Proc. PCIM Eur.*, Nuremberg, Germany, 2015, pp. 1–8.

- [23] T. Negishi, R. Tsuda, K. Ota, S. Iura, and H. Yamaguchi, “3.3 kV all-SiC power module for traction system use,” in *Proc. Europe, Int. Exhib. Conf. Power Electron., Intell. Motion, Renew. Energy Energy Manage. (PCIM)*, Nuremberg, Germany, 2017, pp. 1–6.
- [24] “Mitsubishi electric installs railcar traction system with all-SiC power modules on Shinkansen bullet trains,” Mitsubishi Electric Press Release, Tokyo, Japan, Tech. Rep. 2942, Jun. 2015. [Online]. Available: <https://www.mitsubishielectric.com/news/2015/pdf/0625.pdf>
- [25] T. Ishigaki *et al.*, “3.3 kV/450 a full-SiC nHPD2 (next high power density dual) with smooth switching,” in *Proc. Eur. Int. Exhib. Conf. Power Electron., Intell. Motion, Renew. Energy, Energy Manage. (PCIM)*, Nuremberg, Germany, 2017, pp. 1–6.
- [26] D. Kawase, M. Inaba, K. Horiuchi, and K. Saito, “High voltage module with low internal inductance for next chip generation-next High Power Density Dual (nHPD2),” in *Proc. PCIM Eur.*, 2015, Nuremberg, Germany, 2015, pp. 1–7.
- [27] S. S. Buchholz, M. Wissen, and T. Schuetze, “Electrical performance of a low inductive 3.3kV half bridge IGBT module,” in *Proc. PCIM Eur.*, Nuremberg, Germany, 2015, pp. 1–8.
- [28] *Semikron SEMITRANS 20*. Accessed: Mar. 2020. [Online]. Available: <https://www.semikron.com/about-semikron/news-press/detail/semitrans-20.html/>
- [29] *Wolfspeed 3.3kV SiC XHV-7*. Accessed: Mar. 2020. [Online]. Available: <https://www.wolfspeed.com/pcim-europe-2018/>
- [30] J. C. Balda and A. Mantooth, “Power-semiconductor devices and components for new power converter developments: A key enabler for ultrahigh efficiency power electronics,” *IEEE Power Electron. Mag.*, vol. 3, no. 2, pp. 53–56, Jun. 2016.
- [31] J. W. Palmour *et al.*, “Silicon carbide power MOSFETs: Breakthrough performance from 900 V up to 15 kV,” in *Proc. IEEE 26th Int. Symp. Power Semiconductor Devices IC's (ISPSD)*, Waikoloa, HI, USA, Jun. 2014, pp. 79–82.
- [32] M. Rahimo, “Performance evaluation and expected challenges of silicon carbide power MOSFETs for high voltage applications,” in *Proc. Eur. Conf. Silicon Carbide Rel. Mater. (ECSCRM)*, Halkidiki, Greece, 2016, p. 1.
- [33] N. Iwamuro, “Recent progress of power semiconductor devices and their futures,” in *Proc. IEEE CPMT Symp. Jpn. (ICSJ)*, Kyoto, Japan, Nov. 2017, pp. 191–194.
- [34] D. Aggeler, J. Biela, S. Inoue, H. Akagi, and J. W. Kolar, “Bi-directional isolated DC-DC converter for next-generation power distribution—comparison of converters using Si and SiC devices,” in *Proc. Power Convers. Conf. (Nagoya)*, Nagoya, Japan, Apr. 2007, pp. 510–517.
- [35] J. Fabre, J.-M. Blaquier, A. Verdicchio, P. Ladoux, and S. Sanchez, “Characterization in ZVS mode of SiC MOSFET modules for MVDC applications,” in *Proc. Int. Conf. Clean Electr. Power (ICCEP)*, Otranto, Italy, Jul. 2019, pp. 470–477.
- [36] B. J. Lyons, J. G. Hayes, and M. G. Egan, “Magnetic material comparisons for high-current inductors in low-medium frequency DC-DC converters,” in *Proc. 22nd Annu. IEEE Appl. Power Electron. Conf. Exposit. (APEC)*, Anaheim, CA, USA, Feb. 2007, pp. 71–77.
- [37] G. Ortiz, J. Biela, and J. W. Kolar, “Optimized design of medium frequency transformers with high isolation requirements,” in *Proc. 36th Annu. Conf. IEEE Ind. Electron. Soc. (IECON)*, Glendale, AZ, USA, Nov. 2010, pp. 631–638.
- [38] M. A. Bahmani, T. Thiringer, and M. Kharezy, “Optimization and experimental validation of medium-frequency high power transformers in solid-state transformer applications,” in *Proc. IEEE Appl. Power Electron. Conf. Exposit. (APEC)*, Long Beach, CA, USA, Mar. 2016, pp. 3043–3050.
- [39] J. Kaiser, M. Barwig, and T. Durbbaum, “Novel analysis of the influence of tolerances in geometry and material on the equivalent circuit of a LLC transformer,” in *Proc. PCIM Eur.*, Nuremberg, Germany, 2020, pp. 1803–1810.
- [40] C. Zhao *et al.*, “Power electronic traction transformer—Medium voltage prototype,” *IEEE Trans. Ind. Electron.*, vol. 61, no. 7, pp. 3257–3268, Jul. 2014.
- [41] S. Isler, T. Chaudhuri, D. Aguglia, and X. A. Bonnin, “Development of a 100 kW, 12.5 kV, 22 kHz and 30 kV insulated medium frequency transformer for compact and reliable medium voltage power conversion,” in *Proc. 19th Eur. Conf. Power Electron. Appl. (EPE ECCE Europe)*, Poland, Europe, Sep. 2017, p. 10.
- [42] J. Fabre, P. Ladoux, E. Solano, G. Gateau, and J.-M. Blaquier, “MVDC three-wire supply systems for electric railways: Design and test of a full SiC multilevel chopper,” *IEEE Trans. Ind. Appl.*, vol. 53, no. 6, pp. 5820–5830, Nov. 2017.
- [43] K. Filsoof and P. W. Lehn, “A bidirectional modular multilevel DC-DC converter of triangular structure,” *IEEE Trans. Power Electron.*, vol. 30, no. 1, pp. 54–64, Jan. 2015.
- [44] F. Alhuwaishel, A. Allehyani, S. Al-Obaidi, and P. Enjeti, “A medium voltage DC collection grid for large scale PV power plants with interleaved modular multilevel converter,” *IEEE J. Emerg. Sel. Topics Power Electron.*, vol. 8, no. 4, pp. 3434–3443, Dec. 2020.
- [45] Y. Chen, S. Zhao, Z. Li, X. Wei, and Y. Kang, “Modeling and control of the isolated DC-DC modular multilevel converter for electric ship medium voltage direct current power system,” *IEEE J. Emerg. Sel. Topics Power Electron.*, vol. 5, no. 1, pp. 124–139, Mar. 2017.
- [46] C. Sun, X. Cai, G. Shi, and J. Zhang, “Voltage balancing control of isolated modular multilevel DC-DC converter for use in DC grids with zero voltage switching,” *IET Power Electron.*, vol. 9, no. 2, pp. 270–280, Feb. 2016.
- [47] D. Dujic, A. Mester, T. Chaudhuri, A. Coccia, F. Canales, and J. K. Steinke, “Laboratory scale prototype of a power electronic transformer for traction applications,” in *Proc. 14th Eur. Conf. Power Electron. Appl.*, Birmingham, U.K., 2011, pp. 1–10.
- [48] *Illinois Capacitor—HC5 Series*. Accessed: Mar. 2020. [Online]. Available: <https://www.illinoiscapacitor.com/pdf/seriesDocuments/HC5series.pdf>
- [49] J. Fabre, P. Ladoux, and M. Piton, “Characterization and implementation of dual-SiC MOSFET modules for future use in traction converters,” *IEEE Trans. Power Electron.*, vol. 30, no. 8, pp. 4079–4090, Aug. 2015.
- [50] F. Forest *et al.*, “Use of opposition method in the test of high-power electronic converters,” *IEEE Trans. Ind. Electron.*, vol. 53, no. 2, pp. 530–541, Apr. 2006.



Joseph Fabre was born in Carcassonne, France, in 1985. He received the Engineering degree in electrical engineering from the École Nationale Supérieure d'Électrotechnique, d'Électronique, d'Informatique, d'Hydraulique et des Télécommunications (ENSEEIHT), Toulouse, France, in 2009, and the Ph.D. degree in electrical engineering from the Institut National Polytechnique de Toulouse (INPT), Toulouse, in conjunction with the Traction System Engineering Department, ALSTOM Transport Company, Tarbes, France, in 2013.

From 2014 to 2016, he was a Post-Doctoral Researcher in power electronics research programs for railway applications with the Laboratory on Plasma and Conversion of Energy, University of Toulouse, Toulouse. He is currently still at the Laboratory on Plasma and Conversion of Energy where he is on a mission on behalf of the French National Railway Company (SNCF). He is now involved in research programs on power electronics for railways networks.



Philippe Ladoux (Member, IEEE) was born in France in 1963. He received the Engineering degree in electrical engineering from the École Nationale Supérieure d'Électrotechnique, d'Électronique, d'Informatique, d'Hydraulique et des Télécommunications (ENSEEIHT), Toulouse, France, in 1987, and the Ph.D. degree in electrical engineering from the Institut National Polytechnique de Toulouse, Toulouse, in 1992.

From 2001 to 2009, he was the Manager of the Laboratory on Plasma and Conversion of Energy, Static Converters Research Group, Toulouse. He is currently a Professor with the Institut National Polytechnique de Toulouse, where he teaches power electronics. He is now involved in research programs on power electronics for railway traction. His research interest includes high-power converters.



Hervé Caron was born in Péronne, France, in 1966. He received the B.Sc. degree from the University of Lille, Lille, France, in 1989, and the Expert degree in railway electrification systems from the French National Railway Company (SNCF), Toulouse, France, in 2009.

He has been with SNCF since 1991. Since 2001, he has been with the Institut National Polytechnique of Toulouse, Toulouse, with a focus on high-power converters for railway electrification systems. Since 2017, he has been managing the Project New DC Supply for Railway Electrification.



Andrea Verdicchio was born in San Felice a Cencello, Italy, in 1988. He received the Ph.D. degree in railway electrical engineering from the Institut National Polytechnique of Toulouse, Toulouse, France, in 2019.

He is currently with French National Railway Company (SNCF I&R), Toulouse, where he is also a Junior Researcher in the power supply system and railway smartgrid solutions.



Didier Flumian received the M.Sc. degree in electric engineering from the Conservatoire National des Arts et Métiers, Toulouse, France, in 2003.

Since 2010, he has been an Engineer with the Laboratoire Plasma et Conversion d'Energie, Toulouse. His main works deal with dc-dc converters for high-power and high-performance applications and measurement of losses in power semiconductors and magnetic components.



Jean-Marc Blaquièr received the Engineering degree in electrical engineering from the Conservatoire National des Arts et Métiers (CNAM), Paris, France, in 2001.

He worked on power electronics for several companies from 1988 to 1996. He was with the University of Le Havre, Le Havre, France. Since 2001, he has been a Power Electronics Engineer with the Laboratoire Plasma et Conversion d'Energie, University of Toulouse, Toulouse, France. He designs electronic systems mainly for two research fields: high-power multilevel converters and safe and fault-tolerant operation of converters. He develops test benches of new components and converters for electrical networks (railways, aerospace, and renewable energy). His fields of competence concern electric power distribution (2 kA–3.5 kV), cooling systems, and mechanical integration.



Sébastien Sanchez was born in Toulouse, France, in 1987. He received the M.Sc. degree in electrical engineering from the University of Toulouse, Toulouse, and ENSEEIHT, Toulouse, in 2011, and the Ph.D. degree in electrical engineering from the Institut National Polytechnique of Toulouse (INPT), Toulouse, in 2015.

He joined the ICAM School, Toulouse, in 2015, as an Assistant Professor of electrical engineering. Since 2016, he has been with the Static Converter Group, Laplace laboratory, Toulouse, for his research activities. His main interest includes multicell converters for high-power applications.